NETWORKS AND HETEROGENEOUS MEDIA
©American Institute of Mathematical Sciences
Volume **8**, Number **2**, June **2013**
doi:10.3934/nhm.2013.8.481
pp. **481–499**

DOMAIN PATTERNS AND HYSTERESIS IN PHASE-TRANSFORMING SOLIDS: ANALYSIS AND NUMERICAL SIMULATIONS OF A SHARP INTERFACE DISSIPATIVE MODEL VIA PHASE-FIELD APPROXIMATION

Antonio DeSimone

SISSA–International School for Advanced Studies
via Bonomea 265
34136 Trieste, Italy

Martin Kružík

Institute of Information Theory and Automation, of the ASCR
Pod vodárenskou věží 4
182 08 Prague 8, Czech Republic
Faculty of Civil Engineering, Czech Technical University
Thákurova 7
166 29 Prague, Czech Republic

(Communicated by Benedetto Piccoli)

This paper is dedicated to R. D. James on the occasion of his 60th birthday.

Abstract. We propose a sharp-interface model which describes rate-independent hysteresis in phase-transforming solids (such as shape memory alloys) by resolving explicitly domain patterns and their dissipative evolution. We show that the governing Gibbs' energy functional is the Γ-limit of a family of regularized Gibbs' energies obtained through a phase-field approximation. This leads to the convergence of the solution of the quasistatic evolution problem associated with the regularized energy to the one corresponding to the sharp interface model. Based on this convergence result, we propose a numerical scheme which allows us to simulate mechanical experiments for both spatially homogeneous and heterogeneous samples. We use the latter to assess the role that impurities and defects may have in determining the response exhibited by real samples. In particular, our numerical results indicate that small heterogeneities are essential in order to obtain spatially localized nucleation of a new martensitic variant from a pre-existing one in stress-controlled experiments.

1. **Introduction.** The understanding of hysteresis effects in materials undergoing stress- and/or temperature-induced phase transformations is essential for many engineering applications. Shape memory alloys provide a relevant example. In spite of intense research in the last few decades, however, prediction of hysteresis from fundamental material properties is still a widely open problem. The reader is referred to [26] for an inspiring overview.

2000 *Mathematics Subject Classification.* Primary: 74N30, 49J45, 74D10; Secondary: 74S05.
Key words and phrases. Hysteresis, shape memory alloys, multi-well energies, rate-independent processes, phase-field models, sharp-interface limits.
The second author is supported by GAČR grant P201/12/0671.

Shape memory materials have one high temperature, high symmetry phase called *austenite* and a low temperature, lower symmetry phase called *martensite*. The austenitic phase exists only in one variant while the martensitic phase exists in several symmetry–related variants. Different variants represent different stress-free states of the material and are described by different transformation strains from the parent, high symmetry phase. We are interested in processes where the movement of phase boundaries is rather slow and it is associated with small changes of the external loading on the specimen. This is what typically happens during the stress-induced transformation from austenite to martensite, or during processes involving rearrangement of martensitic variants induced by changes of applied loads or boundary conditions. In all these cases, hysteresis phenomena are pervasive.

There are many phenomenological models describing hysteresis behavior of shape memory alloys, see e.g. [27, 29, 31, 32, 33, 35, 36, 37, 38, 39, 40]. Roughly speaking, the origin of hysteresis in these models is either the nonconvexity of the energy landscape, or a kinetic barrier for the phase transformation, or a combination of these two mechanisms. Models with a "dry friction" type of dissipation provide such a kinetic barrier. They were developed by Mielke and his collaborators in [35, 36, 37] and applied to a wide range of physical phenomena, including wetting on rough surfaces [1, 24, 19]. In dry friction models, the dissipative term, seen as a function of the rate of change of the relevant internal variable, is homogeneous of degree *one*. This results in rate–independent hysteresis even if the energy functional is convex. These models allow for a realistic description of the stored energy of the material (which takes into account its multiwell structure) and for rigorous treatment of coherence and incoherence between various phases. Various numerical aspects are discussed e.g. in [6, 28, 29]

In this paper, we propose a rate-independent model for the dissipative evolution of domain patterns, and a numerical scheme for its solution. We restrict our attention to the case in which only martensitic variants are present, since we have explored only this scenario with our numerical experiments. While conceptually straightforward, generalizations to the study of stress-induced martensite starting from austenite are computationally demanding, and will be considered in future work. In particular, we plan to address the interesting issue of whether kinematic compatibility between austenite and a single variant of martensite is the key to obtain low-hysteresis materials, as suggested in [17].

In our model, sharp interfaces between different phases are allowed and penalized by surface energy. Moreover, within each phase, an elastic energy penalizes deviations of the state of deformation from the stress-free state uniquely associated with that phase. A dissipation term of dry-friction type penalizes phase changes and motion of interfaces between phases.

Our model can be obtained as the sharp interface limit of a dissipative phase-field model. This gives a natural approximation scheme which we use both to prove existence of solutions for the quasi-static evolution problem, and to find them with numerical simulations. A similar phase-field model for martensitic thin films is studied numerically in [41] in the static situation. Phase field approaches to the evolution of microstructures have already been considered in the literature, but they are typically based on rate-dependent, viscous-type dissipative mechanisms such as [17]. See also [30] for a related approach based on a gradient flow, and [10, 13, 14, 15, 16] for studies of rate-independent models (arising in plasticity with softening), their viscous regularization, and their vanishing viscosity limit. We plan

to study the relative merits of rate-dependent versus rate-independent models in future work.

We use our model, and the possibility of performing numerical simulations of mechanical experiments to address the issue of spatially localized nucleation of a martensitic variant from a different pre-existing one. We can reproduce this phenomenon with our model. However, at least for the case of stress-controlled experiments, this requires that we include some heterogeneity in the material properties (random noise in the magnitude of the phase-change penalty term). Our tentative conclusion is that imperfections play a crucial role in making spatial localization possible. This phenomenon is reminiscent of the key role of defects in determining the hysteretic behavior of small ferromagnetic particles [7, 18], and of imperfection sensitivity in the buckling of elastic structures [5, 43]

The rest of the paper is organized as follows. First, we set up our model of a rate-independent evolution with a surface energy assigned to sharp interfaces (Section 2). Then we introduce a phase-field approximation (Section 3) for the governing energy functional, and prove the existence of the so-called energetic solutions for the quasistatic evolution problem. In Section 4, we prove Γ-convergence of the approximate phase-field energy functionals to the original one, and convergence of the corresponding quasistatic evolutions. The construction used for the existence proof and the convergence result suggest a natural numerical algorithm to find solutions of our rate-independent dissipative model, based on solving incremental minimization problems for its phase-field approximation. This is illustrated in Section 5, where the algorithm is applied to some concrete boundary value problems that can be interpreted as numerical simulations of relevant mechanical experiments. In spite of the simplicity of the model used in the numerical simulations, we obtain results that are both plausible and realistic, and closely reminiscent of the striking experimental observations by Chu and James reported, e.g., in [26].

In what follows, $W^{1,2}(\Omega;\mathbb{R}^n)$ will denote a standard Sobolev space of measurable mappings defined on a bounded Lipschitz domain $\Omega \subset \mathbb{R}^n$ which are together with their gradients square integrable and take values in $\mathbb{R}^n$. Further, we will denote by $L^p(\Omega;\mathbb{R}^m)$ standard Lebesgue spaces, by $BV(X;Y)$ a space of mappings with bounded variation defined on X with the target in Y, and $B(0,T;W^{1,2}(\Omega;\mathbb{R}^n))$ will stand for the space of bounded (not necessarily measurable) mappings defined on interval $(0,T)$ with values in $W^{1,2}(\Omega;\mathbb{R}^n)$. Finally, $C^\alpha(X,Y)$ denotes the space of mappings which are $\alpha \geq 0$ times continuously differentiable.

2. **Model description.** We study the quasistatic evolution of a phase-transforming material by using the notion of energetic solution introduced by Mielke and his collaborators [35, 37, 36]. This approach requires the introduction of state variables (in our case displacement u and the vector $\boldsymbol{c}$ describing concentrations of various phases), of a Gibbs energy $\mathcal{I}$ and of a dissipation $\mathcal{D}$. Energetic solutions are processes $t \mapsto (u(t), \boldsymbol{c}(t))$ satisfying the global stability condition and the energy-dissipation balance involving $\mathcal{I}$ and $\mathcal{D}$ given below, cf. (15) and (16). The notion of energetic solution is made precise in Definition 2.1.

We denote by $u : \Omega \to \mathbb{R}^n$ the displacement of a body occupying the region $\Omega \subset \mathbb{R}^n$ in the reference configuration. The infinitesimal strain tensor is

$$e(u) := \frac{1}{2}(\nabla u + (\nabla u)^\top) \ .$$

Decomposing the overall strain into the elastic and transformation ones we have

$$e := e^{\rm el} + e^{\rm tr}$$

where $e^{\rm el}$ is implicitly defined by the constitutive equation for the stress of linear elasticity

$$\sigma(u) := \mathcal{C}(e(u) - e^{\rm tr}) \ , \tag{1}$$

and $\mathcal{C}$ is the fourth–order tensor of elastic constants for which we assume the standard ellipticity condition, i.e., that

$$\exists \gamma > 0 \text{ s.t. } \forall A \in \mathbb{R}^{n\times n} : \sum_{i,j,k,l=1}^{n} \mathcal{C}_{ijkl} A_{ij} A_{kl} \geq \gamma |A|^2 \ . \tag{2}$$

The transformation strain is defined by

$$e^{\rm tr}(\boldsymbol{c}(x)) := \sum_{i=1}^{m} c_i(x) e^{i*} \ , \tag{3}$$

where the symmetric $n \times n$ matrices $\{e^{i*}\}_{i=1}^m$ are the given stress-free strains of m martensite variants and $\boldsymbol{c} = (c_1, \dots, c_m)$ is the vector of the corresponding volume fractions (concentrations) satisfying the obvious conditions

$$\sum_{i=1}^{m} c_i = 1 \ , \ c_i \geq 0 \text{ for all } 1 \leq i \leq m. \tag{4}$$

In the sharp interface model, only pure phases are allowed at each material point. In other words, $\boldsymbol{c}(x)$ can have only one nonzero component at each $x \in \Omega$.

The stored energy density associated with $\sigma(u)$ is

$$W(e, \boldsymbol{c}) := \frac{1}{2} \mathcal{C}(e - e^{\rm tr}(\boldsymbol{c})) \cdot (e - e^{\rm tr}(\boldsymbol{c})) \tag{5}$$

and the corresponding stored elastic energy functional is

$$\mathcal{E}(u, \boldsymbol{c}) := \int_\Omega W(e(u(x)), \boldsymbol{c}(x)) \, {\rm d}x \ . \tag{6}$$

Small–strain, multi–well free–energies of a similar type, and their relation to the corresponding models in the large strain regime are discussed, e.g., in [20].

Besides the elastic energy we also define a surface energy which is the energy stored in the interface between two different phases. This energy is postulated to be

$$\mathcal{S}_0(\boldsymbol{c}) := \frac{1}{2} \sum_{k,l=1}^{m} \varsigma_{kl} \mathcal{H}^{n-1}(\partial^* \{x \in \Omega; \ \boldsymbol{c}(x) = \boldsymbol{c}^{k*}\} \cap \partial^* \{x \in \Omega; \ \boldsymbol{c}(x) = \boldsymbol{c}^{l*}\}) \ , \tag{7}$$

where $\varsigma_{kl} = \varsigma_{lk} \geq 0$, $k, l = 1, \dots m$, is a surface tension coefficient, namely, the energy per unit area of the interface between phases k and l. Clearly, $\varsigma_{kk} = 0$ for all admissible k. Further, $\mathcal{H}^{n-1}$ denotes the $(n-1)$-dimensional Haussdorff measure, $\partial^* A$ denotes the so-called reduced boundary of the set A, see e.g. [21], and $\boldsymbol{c}^{k*} \in \mathbb{R}^m$ is the unit vector with only one nonzero component which is one and is placed at the k-th position

$$(\boldsymbol{c}^{k*})_i := \begin{cases} 1 & \text{if } i = k, \\ 0 & \text{else} \ , \end{cases} \tag{8}$$

hence $\|\boldsymbol{c}\|_{L^1(\Omega;\mathbb{R}^m)}+\mathcal{S}_0(\boldsymbol{c})$ is a norm of $\boldsymbol{c}$ in the space of mappings possesing bounded variation (see e.g. [21]) which we denote $\mathrm{BV}(\Omega;\mathbb{R}^m)$. Altogether, the Helmholtz free–energy reads

$$\mathcal{E}(u,\boldsymbol{c})+\mathcal{S}_0(\boldsymbol{c}) \tag{9}$$

We assume, that a possibly time-dependent displacement u_0 is prescribed on a portion Γ_0 of the boundary $\partial\Omega$ of the specimen. Extensions to cases in which only some components of u_0 are prescribed are straightforward. Evolution is driven by slowly–varying imposed displacements or slowly–varying applied forces. Considering our process time being the interval $[0,T]$ for some $T>0$, the work of surface forces $f_s:[0,T]\times\Gamma_1\to\mathbb{R}^n$ applied on $\partial\Omega\supset\Gamma_1$ at a time $t\in[0,T]$ and the work of body forces with density $f:[0,T]\times\Omega\to\mathbb{R}^n$ can be expressed through

$$\mathcal{L}(t,u):=\int_{\Gamma_1} f_s(t,x)\cdot u(x)\,\mathrm{d}S+\int_\Omega f(t,x)\cdot u(x)\,\mathrm{d}x\ . \tag{10}$$

We assume that $\Gamma_0\cap\Gamma_1=\emptyset$.

Thus, the total Gibbs energy of the specimen at $t\in[0,T]$ has the form

$$\mathcal{I}(t,u,\boldsymbol{c}):=\mathcal{E}(u,\boldsymbol{c})+\mathcal{S}_0(\boldsymbol{c})-\mathcal{L}(t,u)\ . \tag{11}$$

As the system evolves it may also dissipate some energy. We associate the dissipation with the magnitude of the time derivative of $\boldsymbol{c}$. This makes the evolution rate-independent and therefore independent of the loading rate. We define the dissipation rate per unit volume as

$$\varrho(x,\dot{\boldsymbol{c}}):=g(x)|\dot{\boldsymbol{c}}|_m\ , \tag{12}$$

where $|\boldsymbol{c}|_m:=\sum_{i=1}^m\alpha_i|c_i|$, and $\alpha_i>0$, and $g\geq 0$. Then $g(x)\alpha_i$ is the specific energy which is dissipated if c_i changes from either zero to one or from one to zero at the material point $x\in\Omega$. For this reason we refer to g as the magnitude of the energy penalty for phase change, or *penalty function* for brevity. The possibility of assuming a non-constant, randomly modulated function $g(x)$ representing random heterogeneities or defects will play an important role in the simulation of stress-controlled experiments in Section 5.2.

The specific dissipated energy associated with a change of the volume fractions from $\boldsymbol{c}$ to $\tilde{\boldsymbol{c}}$ is therefore

$$D(x,\boldsymbol{c},\tilde{\boldsymbol{c}}):=g(x)|\boldsymbol{c}-\tilde{\boldsymbol{c}}|_m \tag{13}$$

and the total dissipation reads

$$\mathcal{D}(\boldsymbol{c},\tilde{\boldsymbol{c}}):=\int_\Omega D(x,\boldsymbol{c}(x),\tilde{\boldsymbol{c}}(x))\,\mathrm{d}x\ .$$

We write $(u,\boldsymbol{c})\in\mathbb{Q}$, where $\mathbb{Q}:=\mathbb{U}\times\mathbb{C}$ and $\mathbb{U}$ and $\mathbb{C}$ are specified below, to indicate that a pair $(u,\boldsymbol{c})$ is an admissible state for our system. As we expect spatial jumps in $\boldsymbol{c}$, we set $\mathbb{C}:=\{\boldsymbol{c}\in BV(\Omega;\mathbb{R}^m);\ \tilde{\Phi}(\boldsymbol{c})=0\}$ with

$$\tilde{\Phi}(\boldsymbol{c}):=\begin{cases}0 \text{ if } \boldsymbol{c}=\boldsymbol{c}^{k*} \text{ for some } k\in\{1,\dots,m\}\\ >0 \text{ otherwise.}\end{cases} \tag{14}$$

In case of time-independent Dirichlet boundary conditions, we set $\mathbb{U}:=\{u\in W^{1,2}(\Omega;\mathbb{R}^n);\ u=u_0 \text{ on } \Gamma_0\}$ while if $u_0(t)\in W^{1,2}(\Omega;\mathbb{R}^n)$ for all $t\in[0,T]$ we take $\mathbb{U}:=\{v\in W^{1,2}(\Omega;\mathbb{R}^n); v=0 \text{ on } \Gamma_0\}$ and we work with the energy functional of the form $t\mapsto\mathcal{I}(t,v(t)+u_0(t),\boldsymbol{c}(t))$ where $v(t)\in\mathbb{U}$. This makes the set of admissible states $\mathbb{Q}$ independent of time.

The following two properties are the key ingredients in the definition of energetic solution of a rate-independent dissipative process see [35, 37, 36].
(i) Global Stability Inequality:
We say that $t \mapsto (u(t), \boldsymbol{c}(t)) \in \mathbb{Q}$ is stable if, $\forall t \in [0,T]$ and $\forall (\tilde{u}, \tilde{\boldsymbol{c}}) \in \mathbb{Q}$, one has

$$\mathcal{I}(t, u(t), \boldsymbol{c}(t)) \leq \mathcal{I}(t, \tilde{u}, \tilde{\boldsymbol{c}}) + \mathcal{D}(\boldsymbol{c}(t), \tilde{\boldsymbol{c}}) \ . \tag{15}$$

(ii) Energy-Dissipation Balance:
We say that $t \mapsto (u(t), \boldsymbol{c}(t))$ satisfies the energy–dissipation balance if $\forall\ 0 \leq t \leq T$

$$\mathcal{I}(t, u(t), \boldsymbol{c}(t)) + \mathrm{Var}(\mathcal{D}, \boldsymbol{c}; [0,t]) = \mathcal{I}(0, u_0, \boldsymbol{c}_0) + \int_0^t \frac{\partial}{\partial t} \mathcal{I}(\xi, u(\xi), \boldsymbol{c}(\xi))\, \mathrm{d}\xi \ , \tag{16}$$

where

$$\mathrm{Var}(\mathcal{D}, \boldsymbol{c}; [0,t]) := \sup \left\{ \sum_{i=1}^{N} \mathcal{D}(\boldsymbol{c}(t_i), \boldsymbol{c}(t_{i-1})); \ \{t_i\} \text{ any partition of } [0,t] \right\} \ .$$

We denote the set of stable states at the time t by $S(t)$, i.e.,

$$S(t) := \{(u, \boldsymbol{c}) \in \mathbb{Q};\ \forall (\tilde{u}, \tilde{\boldsymbol{c}}) \in \mathbb{Q};\ \mathcal{I}(t, u, \boldsymbol{c}) \leq \mathcal{I}(t, \tilde{u}, \tilde{\boldsymbol{c}}) + \mathcal{D}(\boldsymbol{c}, \tilde{\boldsymbol{c}})\} \ . \tag{17}$$

Definition 2.1. The mapping $t \mapsto (u(t), \boldsymbol{c}(t)) \in \mathbb{Q}$ is an energetic solution to problem $(\mathcal{I}, \mathcal{D})$ with an initial condition $(u(0), \boldsymbol{c}(0)) = (u^0, \boldsymbol{c}^0) \in S(0)$, namely, the quasistatic evolution problem governed by energy $\mathcal{I}$ and dissipation $\mathcal{D}$, if the stability inequality (15) and the energy–dissipation balance (16) are satisfied for all $t \in [0,T]$.

Following [25], we further assume that there are constants $C_0, C_1 > 0$ such that

$$|\partial_t \mathcal{I}(t, u, \boldsymbol{c})| \leq C_0 (C_1 + \mathcal{I}(t, u, \boldsymbol{c})) \ . \tag{18}$$

As a consequence we have

$$\mathcal{I}(t_2, u, \boldsymbol{c}) \leq (C_1 + \mathcal{I}(t_1, u, \boldsymbol{c})) \exp(C_0 |t_2 - t_1|) - C_1 \ . \tag{19}$$

Further we assume uniform continuity of $t \mapsto \partial_t \mathcal{I}(t, u, \boldsymbol{c})$ in the sense that there exists $\omega : [0,T] \to [0, +\infty)$ nondecreasing, such that for all $t_1, t_2 \in [0,T]$

$$|\partial_t \mathcal{I}(t_1, u, \boldsymbol{c}) - \partial_t \mathcal{I}(t_2, u, \boldsymbol{c})| \leq \omega(|t_1 - t_2|) \ . \tag{20}$$

We also suppose that $(u, \boldsymbol{c}) \mapsto \partial_t \mathcal{I}(t, u, \boldsymbol{c})$ is weakly continuous for all $t \in [0,T]$.

Remark 1. In the case when $t \mapsto \boldsymbol{c}(t)$ is smooth and the surface energy is neglected, the notion of energetic solution given above generalizes the classical evolution laws of generalized standard materials [23]. These are the equilibrium conditions

$$\mathrm{div} \sigma = f \text{ in } \Omega \ , \tag{21}$$

$$\sigma \nu = f_s \text{ on } \Gamma_1 \ , \tag{22}$$

where ν is the outer unit normal to $\partial\Omega \supset \Gamma_1$ and the flow rule

$$-\frac{\partial W(e, \boldsymbol{c})}{\partial \boldsymbol{c}} \in \partial \varrho(\cdot, \dot{\boldsymbol{c}}) \ , \tag{23}$$

see [25]. The notion of energetic solution generalizes this framework to processes that may experience time discontinuities, and are governed by nonsmooth energies such as $\mathcal{S}_0$.

In order to prove the existence of an energetic solution to $(\mathcal{I},\mathcal{D})$ we introduce its phase-field approximation with smooth interfaces between various phases. Then we show by a Γ-convergence argument that suitably defined energetic solutions to these approximations converge to an energetic solution of $(\mathcal{I},\mathcal{D})$.

3. **The phase-field approximation.** The main idea of the phase approximation is to replace the term $\mathcal{S}_0$ in the definition of $\mathcal{I}$ in (11) by a more regular term, namely by

$$\int_\Omega \varepsilon|\nabla \boldsymbol{c}(x)|^2 + \frac{\Phi(\boldsymbol{c}(x))}{\varepsilon}\,\mathrm{d}x\ , \tag{24}$$

where $\Phi : \mathbb{R}^m \to [0;+\infty)$,

$$\Phi(\boldsymbol{c}) := \left(\sum_{i=1}^m c_i - 1\right)^2 + \tilde{\Phi}(\boldsymbol{c})$$

and recall that

$$\tilde{\Phi}(\boldsymbol{c}) := \begin{cases} 0 \text{ if } \boldsymbol{c} = \boldsymbol{c}^{k*} \text{ for some } k \in \{1,\dots,m\} \\ > 0 \text{ otherwise.} \end{cases} \tag{25}$$

Thus, we define the surface energy $\mathcal{S}_\varepsilon : L^1(\Omega;\mathbb{R}^m) \to [0;+\infty]$ by

$$\mathcal{S}_\varepsilon(\boldsymbol{c}) := \begin{cases} \int_\Omega \varepsilon|\nabla \boldsymbol{c}(x)|^2 + \frac{1}{\varepsilon}\Phi(\boldsymbol{c}(x))\,\mathrm{d}x \text{ if } \boldsymbol{c} \in W^{1,2}(\Omega;\mathbb{R}^m)\ ,\ \boldsymbol{c} \in [0,1]^m\ , \\ +\infty \text{ otherwise.} \end{cases} \tag{26}$$

Moreover, we define for every $\varepsilon > 0$ the Gibbs energy as

$$\mathcal{I}_\varepsilon(t,u,\boldsymbol{c}) := \mathcal{E}(u,\boldsymbol{c}) + \mathcal{S}_\varepsilon(\boldsymbol{c}) - \mathcal{L}(t,u)\ , \tag{27}$$

$$\mathbb{Q}_{\mathrm{app}} := \mathbb{U} \times L^1(\Omega;\mathbb{R}^m)\ .$$

Having a time interval $[0,T]$ for $T > 0$ we can define an energetic solution to $(\mathcal{I}_\varepsilon,\mathcal{D})$ as a mapping $[0,T] \to \mathbb{Q}_{\mathrm{app}} : t \mapsto (u_\varepsilon(t),\boldsymbol{c}_\varepsilon(t))$. This energetic solution is again defined by means of stability and energy equality as in (15) and (16) with $\mathcal{I}_\varepsilon$, and $\mathbb{Q}_{\mathrm{app}}$ instead of $\mathcal{I}$ and $\mathbb{Q}$, respectively.

Proposition 1. *Let $\varepsilon > 0$ and assume that $f \in C^1([0,T];L^{\tilde{d}}(\Omega;\mathbb{R}^n))$ and $f_s \in C^1([0,T];L^{\hat{d}}(\Gamma_1;\mathbb{R}^n))$ where $\tilde{d} = 6/5$ and $\hat{d} = 4/3$ if $n = 3$ and $\tilde{d},\hat{d} > 1$ if $1 \le n \le 2$. Let the initial condition $(u^0,\boldsymbol{c}^0) \in \mathbb{Q}_{\mathrm{app}}$ be stable. Then there exists an energetic solution $(u_\varepsilon(t,\cdot),\boldsymbol{c}_\varepsilon(t,\cdot)) \in \mathbb{Q}_{\mathrm{app}}$ to $(\mathcal{I}_\varepsilon,\mathcal{D})$ with and $\boldsymbol{c}_\varepsilon(0,\cdot) = \boldsymbol{c}^0$ such that $u_\varepsilon \in B((0,T);W^{1,2}(\Omega;\mathbb{R}^n))$, $\boldsymbol{c}_\varepsilon \in L^\infty((0,T);W^{1,2}(\Omega;\mathbb{R}^m)) \cap BV((0,T);L^1(\Omega;\mathbb{R}^m))$.*

Proof. The proof can be obtained following the one of [25, Th. 3.4]. Here we only sketch it in a few steps for the reader's convenience.
Step 1: Consider a partition $0 = t_\tau^0 < t_\tau^1 < \ldots < t_\tau^N = T$, set $\tau = \max_i(t_i - t_{i-1})$ and suppose that the partition for $N+1$ is a refinement of the partition with N time steps. Take an initial condition $(u^0,\boldsymbol{c}^0) \in \mathbb{Q}_{\mathrm{app}}$. we define the following sequence of minimization problems For $k = 1,\dots,N$ solve

$$\min_{(u,\boldsymbol{c})\in\mathbb{Q}_{\mathrm{app}}} \mathcal{I}_\varepsilon(t_\tau^k,u,\boldsymbol{c}) + \mathcal{D}(\boldsymbol{c}_\tau^{k-1},\boldsymbol{c}) \tag{28}$$

and denote a solution by $(u_\tau^k,\boldsymbol{c}_\tau^k)$. The existence of a solution is a standard application of the direct method of the Calculus of Variations.

Step 2: Solutions (28) are stable. Moreover, it holds that

$$\int_{t_\tau^{k-1}}^{t_\tau^k} \partial_t \mathcal{I}_\varepsilon(s, u_\tau^k, \boldsymbol{c}_\tau^k)\,\mathrm{d}s \le \mathcal{I}_\varepsilon(t_\tau^k, u_\tau^k, \boldsymbol{c}_\tau^k) + \mathcal{D}(\boldsymbol{c}_\tau^{k-1}, \boldsymbol{c}_\tau^k) - \mathcal{I}_\varepsilon(t_\tau^{k-1}, u_\tau^{k-1}, \boldsymbol{c}_\tau^{k-1}) \quad (29)$$
$$\le \int_{t_\tau^{k-1}}^{t_\tau^k} \partial_t \mathcal{I}_\varepsilon(s, u_\tau^{k-1}, \boldsymbol{c}_\tau^{k-1})\,\mathrm{d}s\ .$$

Take $(\tilde{u}, \tilde{\boldsymbol{c}}) \in \mathbb{Q}_{\rm app}$. We have $\mathcal{I}_\varepsilon(t_\tau^k, u_\tau^k, \boldsymbol{c}_\tau^k) + \mathcal{D}(\boldsymbol{c}_\tau^{k-1}, \boldsymbol{c}_\tau^k) \le \mathcal{I}_\varepsilon(t_\tau^k, \tilde{u}, \tilde{\boldsymbol{c}}) + \mathcal{D}(\tilde{\boldsymbol{c}}, \boldsymbol{c}_\tau^{k-1})$. We further estimate $\mathcal{D}(\tilde{\boldsymbol{c}}, \boldsymbol{c}_\tau^{k-1}) - \mathcal{D}(\boldsymbol{c}_\tau^{k-1}, \boldsymbol{c}_\tau^k) \le \mathcal{D}(\tilde{\boldsymbol{c}}, \boldsymbol{c}_\tau^k)$, which proves the stability. The upper estimate in (29) follows by checking minimality of q_τ^k against q_τ^{k-1}, i.e.

$$\begin{aligned}\mathcal{I}_\varepsilon(t_\tau^k, u_\tau^k, \boldsymbol{c}_\tau^k) + \mathcal{D}(\boldsymbol{c}_\tau^k, \boldsymbol{c}_\tau^{k-1}) \quad &\le \quad \mathcal{I}_\varepsilon(t_\tau^k, u_\tau^{k-1}, \boldsymbol{c}_\tau^{k-1}) = \mathcal{I}_\varepsilon(t_\tau^{k-1}, u_\tau^{k-1}, \boldsymbol{c}_\tau^{k-1}) \\ &+ \quad \int_{t_\tau^{k-1}}^{t_\tau^k} \partial_t \mathcal{I}_\varepsilon(s, u_\tau^{k-1}, \boldsymbol{c}_\tau^{k-1})\,\mathrm{d}s\ . \end{aligned} \quad (30)$$

The lower estimate in (29) is implied by the stability of q_τ^{k-1}, namely

$$\begin{aligned}&\mathcal{I}_\varepsilon(t_\tau^{k-1}, u_\tau^{k-1}, \boldsymbol{c}_\tau^{k-1}) \le \mathcal{I}_\varepsilon(t_\tau^{k-1}, u_\tau^k, \boldsymbol{c}_\tau^k) + \mathcal{D}(\boldsymbol{c}_\tau^{k-1}, \boldsymbol{c}_\tau^k) \\ &= \mathcal{I}_\varepsilon(t_\tau^k, u_\tau^k, \boldsymbol{c}_\tau^k) + \mathcal{D}(\boldsymbol{c}_\tau^{k-1}, \boldsymbol{c}_\tau^k) - \int_{t_\tau^{k-1}}^{t_\tau^k} \partial_t \mathcal{I}_\varepsilon(s, u_\tau^k, \boldsymbol{c}_\tau^k)\,\mathrm{d}s\ . \end{aligned} \quad (31)$$

Then define piecewise constant interpolants constructed from $\{(u^k, \boldsymbol{c}^k)\}_k$ and denote them by $(u_\tau^N, \boldsymbol{c}_\tau^N)$. In particular, we define

$$(u_\tau^N(t), \boldsymbol{c}_\tau^N(t)) := (u_\tau^{k-1}, \boldsymbol{c}_\tau^{k-1}) \text{ if } t \in [t_\tau^{k-1}, t_\tau^k)\ ,\ (u_\tau(T), \boldsymbol{c}_\tau(T)) := (u_\tau^N, \boldsymbol{c}_\tau^N)\ . \quad (32)$$

Using (18), (20) and (29) which are also valid for $\mathcal{I}_\varepsilon$ we get the following apriori bounds which are independent of τ:

$$\|u_\tau^N\|_{L^\infty((0,T);W^{1,2}(\Omega;\mathbb{R}^n))} \le C\ ,$$

$$\|\boldsymbol{c}_\tau^N\|_{L^\infty((0,T);W^{1,2}(\Omega;\mathbb{R}^m))} \le C\ ,$$

and

$$\mathrm{Var}(\mathcal{D}, \boldsymbol{c}_\tau^N; [0,T]) \le C\ .$$

Step 3: The existence of an energetic solution is now obtained by passing to the limit for $N \to \infty$ (as the time discretization is refined) in the energy inequality proved in Step 2 and checking the stability of the limit. Notice that the dissipation functional $\mathcal{D} : \mathbb{C} \to \mathbb{R}$ is sequentially continuous with respect to the weak $W^{1,2}(\Omega;\mathbb{R}^m)$ topology. □

If we look at the optimality conditions for problem (28) we get that

$$-\frac{\partial W(e, \boldsymbol{c})}{\partial c_i} - \frac{1}{\varepsilon}\frac{\partial \Phi(\boldsymbol{c})}{\partial c_i} - 2\varepsilon\Delta c_i \in \partial_{c_i}\varrho(x, \boldsymbol{c} - \boldsymbol{c}_\tau^{k-1})\,, \quad i = 1, \dots, m\,. \quad (33)$$

So, in view of (12) a phase change $\boldsymbol{c}_\tau^k \neq \boldsymbol{c}_\tau^{k-1}$ occurs if

$$\sigma(u) \cdot e^{i*} + \frac{1}{\varepsilon}\frac{\partial \Phi(\boldsymbol{c})}{\partial c_i} + 2\varepsilon\Delta c_i = \pm g\alpha_i \quad (34)$$

for some $i \in \{1, \dots, m\}$, where $\sigma(u)$ is given by (1).

4. **The sharp interface limit** $\varepsilon \to 0$**.** We showed in the previous section that there is an energetic solution for every $\varepsilon > 0$. The aim of this section is to study the limiting problem as $\varepsilon \to 0$. We first find out the corresponding energy functional and then show in what sense solutions for $\varepsilon > 0$ approximate the limit one. The main tool of our analysis will be the notion of Γ-convergence [12].

Convergence of energetic solutions to problems $(\mathcal{I}_\varepsilon, \mathcal{D})$ to an energetic solution solving the problem $(\mathcal{I}, \mathcal{D})$, where $\mathcal{I}$ is the the Gamma-limit of the energy $\mathcal{I}_\varepsilon$ follows from the work of Mielke, Roubíček, and Stefanelli [34]. It is, however, important to define the surface tension coefficients $\{\varsigma_{kl}\}$ in the definition of $\mathcal{S}_0$ and to link them to the function Φ. For this, we define the distance between two variants (vector volume fractions) $\boldsymbol{c}_1$ and $\boldsymbol{c}_2$ of the material as

$$d(\boldsymbol{c}_1, \boldsymbol{c}_2) := \inf \big\{ 2 \int_{-1}^{1} \sqrt{\Phi(\gamma(t))} |\gamma'(t)| \mathrm{d}t;\ \gamma \in C^{0,1}([-1;1]; \mathbb{R}^m) \\ ,\ \gamma(-1) = \boldsymbol{c}_1 \,, \gamma(1) = \boldsymbol{c}_2 \big\} \,,$$

where $C^{0,1}([-1,1]; \mathbb{R}^m)$ denotes the space of Lipschitz maps $\gamma : [-1,1] \to \mathbb{R}^m$. Hence, γ' is defined almost everywhere in $[-1,1]$. Then the surface tension coefficients are defined as $\varsigma_{kl} := d(\boldsymbol{c}^{k*}, \boldsymbol{c}^{l*})$ for all $k, l \in \{1, \dots, M\}$. Thus, we see that clearly, $\varsigma_{kl} = \varsigma_{lk}$ and that $\varsigma_{kk} = 0$.

We will further assume that there are positive $\alpha, \beta \in \mathbb{R}$ such that

$$\Phi(\boldsymbol{c}) \geq \alpha |\boldsymbol{c}|^2 - \beta \,. \tag{35}$$

Let us finally set the surface energy $\mathcal{S} : L^1(\Omega; \mathbb{R}^m) \to [0, +\infty]$

$$\mathcal{S}(\boldsymbol{c}) := \begin{cases} \mathcal{S}_0(\boldsymbol{c}) \text{ if } \boldsymbol{c} \in \mathrm{BV}(\Omega; \mathbb{R}^m) \text{ and } \Phi(\boldsymbol{c}) = 0 \text{ a.e. in } \Omega \\ +\infty \text{ otherwise.} \end{cases} \tag{36}$$

Proposition 2. *Assume that (35) and (2) are satisfied. Then the following holds.*
(i) Let $\{u_\varepsilon, \boldsymbol{c}_\varepsilon\}_{\varepsilon>0} \subset \mathbb{Q}_{\mathrm{app}}$ *be such that* $\mathcal{E}(u_\varepsilon, \boldsymbol{c}_\varepsilon) + \mathcal{S}_\varepsilon(\boldsymbol{c}_\varepsilon) < C$ *for some* $C > 0$. *Then there exists a subsequence* $\{\varepsilon_k\}_{k \in \mathbb{N}}$ *converging to zero as* $k \to \infty$, $u \in \mathbb{U}$ *and* $\boldsymbol{c} \in \mathrm{BV}(\Omega; \mathbb{R}^m) \cap L^2(\Omega; \mathbb{R}^m)$ *such that* $\lim_{k\to\infty} \boldsymbol{c}_{\varepsilon_k} = \boldsymbol{c}$ *in* $L^2(\Omega; \mathbb{R}^m)$ *and* $\text{weak-}\lim_{k\to\infty} u_{\varepsilon_k} = u$ *in* $W^{1,2}(\Omega; \mathbb{R}^n)$. *Moreover,* $\boldsymbol{c} \in \{\boldsymbol{c}^{1*}, \dots \boldsymbol{c}^{m*}\}$ *almost everywhere in* Ω.
(ii) For every $(u_{\varepsilon_k}, \boldsymbol{c}_{\varepsilon_k})_k \in \mathbb{Q}_{\mathrm{app}}$ *such that* $u_{\varepsilon_k} \to u$ *in* $L^2(\Omega; \mathbb{R}^n)$ *and* $\boldsymbol{c}_{\varepsilon_k} \to c$ *in* $L^1(\Omega; \mathbb{R}^m)$ *strongly as* $k \to \infty$ *and* $u \in \mathbb{U}$ *it holds that*

$$\mathcal{E}(u, \boldsymbol{c}) + \mathcal{S}(\boldsymbol{c}) \leq \liminf_{k\to\infty} \mathcal{E}(u_{\varepsilon_k}, \boldsymbol{c}_{\varepsilon_k}) + \mathcal{S}_{\varepsilon_k}(\boldsymbol{c}_{\varepsilon_k}) \,. \tag{37}$$

(iii) For every $\boldsymbol{c} \in L^1(\Omega; \mathbb{R}^m)$ *with nonnegative components and every* $u \in \mathbb{U}$ *there is* $(\tilde{u}_{\varepsilon_k}, \tilde{\boldsymbol{c}}_{\varepsilon_k})_k \in W^{1,2}(\Omega; \mathbb{R}^m)$ *such that* $\tilde{u}_{\varepsilon_k} \to u$ *in* $L^2(\Omega; \mathbb{R}^n)$ *and* $\tilde{\boldsymbol{c}}_{\varepsilon_k} \to \boldsymbol{c}$ *in* $L^1(\Omega; \mathbb{R}^m)$ *as* $k \to \infty$ *and*

$$\mathcal{E}(u, \boldsymbol{c}) + \mathcal{S}(\boldsymbol{c}) \geq \limsup_{k\to\infty} \mathcal{E}_{\varepsilon_k}(\tilde{u}_{\varepsilon_k}, \tilde{\boldsymbol{c}}_{\varepsilon_k}) + \mathcal{S}_{\varepsilon_k}(\tilde{\boldsymbol{c}}_{\varepsilon_k}) \,. \tag{38}$$

Proof. The proof follows the same lines as the proof of Th. 5.1. in [22], therefore we only sketch it. Let us start with (i): As $\mathcal{E}(u_\varepsilon, \boldsymbol{c}_\varepsilon) + \mathcal{S}_\varepsilon(\boldsymbol{c}_\varepsilon) < C$ we have that

$$\mathcal{S}_\varepsilon(\boldsymbol{c}_\varepsilon(x)) = \int_\Omega \frac{1}{\varepsilon} \Phi(\boldsymbol{c}_\varepsilon(x)) + \varepsilon |\nabla \boldsymbol{c}_\varepsilon(x)|^2 \,\mathrm{d}x < C \,. \tag{39}$$

We define for $k = 1, \dots, m$ $\phi_k(\boldsymbol{c}) := d(\boldsymbol{c}, \boldsymbol{c}^{k*})$. These are locally Lipschitz functions [2] with $|\nabla \phi_k(\boldsymbol{c})| \leq 2\sqrt{\Phi(\boldsymbol{c})}$. Define $h^k_\varepsilon(x) := \min(\phi_k(\boldsymbol{c}_\varepsilon(x)), 1)$. Applying Young's

inequality we estimate $|\nabla h^k_\varepsilon| \le \varepsilon|\nabla \boldsymbol{c}|^2 + \frac{1}{\varepsilon}\Phi(\boldsymbol{c})$ a.e. in Ω. In view of (39) it shows that $\{h^k_\varepsilon\}_\varepsilon$ is bounded in $\mathrm{BV}(\Omega)$ for all $k = 1, \dots, m$. Hence, we can extract a subsequence $\{\varepsilon_j\}$ tending to zero if $j \to \infty$ such that for all $1 \le k \le m$ $h^k_{\varepsilon_j} \to h^k$ in $L^1(\Omega)$ and almost everywhere in Ω as $j \to \infty$. For all admissible k, the functions h^k are defined just by this limit.

We also see from (39) that $\Phi(\boldsymbol{c}_{\varepsilon_j}) \to 0$ in $L^1(\Omega)$ and therefore also almost everywhere in Ω for a (not relabeled) subsequence. This means that $\boldsymbol{c}_{\varepsilon_j} \to \boldsymbol{c}$, where $\boldsymbol{c}$ only takes values in $\{\boldsymbol{c}^{1*}, \dots, \boldsymbol{c}^{m*}\}$. It follows from (39) that this convergence is even strong in $L^2(\Omega)$. We denote Ω_k a part of Ω where $\boldsymbol{c}$ attains the value $\boldsymbol{c}^{k*}$. It holds that $\Omega = \cup_{k=1}^m \Omega_k \cup N$ where N has the zero Lebesgue measure. Finally, Korn's inequality and (2) imply that $\{u_{\varepsilon_j}\}_j$ is also bounded in $W^{1,2}(\Omega; \mathbb{R}^n)$.

Proof of (ii): We can assume that $\liminf_{k\to\infty} \mathcal{E}(u_{\varepsilon_k}, \boldsymbol{c}_{\varepsilon_k}) + \mathcal{S}_{\varepsilon_k}(\boldsymbol{c}_{\varepsilon_k}) < +\infty$ because otherwise the assertion is trivial. Moreover, assume that $\boldsymbol{c}_\varepsilon \to \boldsymbol{c}$ a.e. in Ω. The coercivity implies that $\int_\Omega \frac{1}{\varepsilon}\Phi(\boldsymbol{c}_\varepsilon(x)) + \varepsilon|\nabla \boldsymbol{c}_\varepsilon(x)|^2 \,\mathrm{d}x < C$, hence $\int_\Omega \Phi(\boldsymbol{c}_\varepsilon(x))\,\mathrm{d}x \to 0$ and $\Phi(\boldsymbol{c}_{\varepsilon_j}) \to 0$ a.e. in Ω for a subsequence. So, $\boldsymbol{c} \in \{\boldsymbol{c}^{1*}, \dots, \boldsymbol{c}^{m*}\}$ almost everywhere in Ω. After some technical manipulation, one can show that for all $1 \le k \le m$ sets $\Omega_k := \{x \in \Omega; \boldsymbol{c} = \boldsymbol{c}^{k*}\}$ has a finite perimeter. The growth conditions on Φ and Korn's inequality ensure that $\boldsymbol{c}_{\varepsilon_j} \to \boldsymbol{c}$ in $L^2(\Omega; \mathbb{R}^m)$ and that $u_{\varepsilon_j} \rightharpoonup u$ in $W^{1,2}(\Omega; \mathbb{R}^n)$ as $j \to \infty$. Finally, it follows that $\mathcal{E}(u, \boldsymbol{c}) \le \liminf_{j\to\infty} \mathcal{E}(u\varepsilon_j, \boldsymbol{c}_{\varepsilon_j})$ and that $\mathcal{S}(\boldsymbol{c}) \le \liminf_{k\to\infty} \mathcal{S}_{\varepsilon_k}(\boldsymbol{c}_{\varepsilon_k})$.

To prove (iii) we rely on the result of [3]; see. also [4, 42] for constructions of the recovery sequence $\boldsymbol{c}_\varepsilon\}_\varepsilon \in W^{1,2}(\Omega; \mathbb{R}^m)$ converging to a given $\boldsymbol{c} \in \mathrm{BV}(\Omega; \mathbb{R}^m)$. Then $(u, \boldsymbol{c}_\varepsilon)$ is the sought sequence realizing the limsup condition. □

Remark 2. Proposition 2 above shows that $\mathcal{E} + \mathcal{S}$ is the Γ-limit of $\mathcal{E} + \{\mathcal{S}_\varepsilon\}$ with respect to the weak $W^{1,2}(\Omega; \mathbb{R}^m)$ convergence of displacements and strong $L^1(\Omega; \mathbb{R}^m)$ convergence of compositions. Since $\mathcal{L}$ is a continuous perturbation with respect to these topologies, we also have

$$\mathcal{I}_\varepsilon \to \mathcal{I} \tag{40}$$

in the sense of Gamma-convergence.

Using Theorem 3.1 in [34], and in view of (40), we have that quasistatic evolutions solving problem $(\mathcal{J}_\varepsilon, \mathcal{D}, \mathcal{L})$ converge to solutions of problem $(\mathcal{J}_0, \mathcal{D}, \mathcal{L})$ as $\varepsilon \to 0$. The precise statement in the following proposition.

Proposition 3. *Let $f \in C^1([0,T]; L^{\tilde{d}}(\Omega; \mathbb{R}^n))$ $f_s \in C^1([0,T]; L^{\hat{d}}(\Gamma_1; \mathbb{R}^n))$ where $\tilde{d} = 6/5$ and $\hat{d} = 4/3$ if $n = 3$ and $\tilde{d}, \hat{d} > 1$ if $1 \le n \le 2$. Let $u_\varepsilon, \boldsymbol{c}_\varepsilon \in \mathbb{Q}_{\mathrm{app}}$ be an energetic solution to problem $(\mathcal{I}_\varepsilon, \mathcal{D})$*

Assume that for almost all $t \in [0,T]$ $u_\varepsilon(t) \to u(t)$ weakly in $W^{1,2}(\Omega; \mathbb{R}^m)$ and for all $t \in [0,T]$ $\boldsymbol{c}_\varepsilon(t) \to \boldsymbol{c}(t) \in L^1(\Omega; \mathbb{R}^m))$ strongly. Let, moreover,

$$\lim_{\varepsilon\to 0} \mathcal{I}_\varepsilon(0, u_\varepsilon(0), \boldsymbol{c}_\varepsilon(0)) \to \mathcal{I}(0, u(0), \boldsymbol{c}(0)) \ .$$

Then $(u, \boldsymbol{c}) \in \mathbb{Q}$ is an energetic solution to $(\mathcal{I}, \mathcal{D})$.

Proof. The result follows from [34, Thm. 3.1]. In view of [34, Lemma 2.1] we need to show the so-called upper semicontinuity of stable sets. Notice that the only term which depends on ε is the elastic energy functional. Hence, it is enough to verify condition (2.19) in [34]. However, this condition follows from the continuity of the dissipation with respect to the strong L^1 topology. □

5. **Numerical simulations.** The constructive proof of existence of solutions for the phase-field approximation (Proposition 1), together with the result showing convergence of the phase-field to the sharp interface model (Proposition 3), suggest a natural approximation scheme for our sharp interface model. This will be based on solving an incremental minimization problems for the phase-field approximation, in which the parameter ε will be fixed at some suitably small value.

We set $\varepsilon = 10^{-6}$, $T = 1$, and perform numerical experiments using a finite element approximation of the phase field problem. To this aim we take $m = 2$, a rectangular domain $\Omega = (0,1) \times (0,2) \subset \mathbb{R}^2$, and discretize it into triangular elements belonging to $\mathcal{T}_h = \{\omega \subset \Omega;\ \text{diam}\ \omega \leq h\}$ such that $\Omega = \cup_{\omega \in \mathcal{T}_h} \omega$. The displacement field u as well as the vector volume fraction $\boldsymbol{c}$ is approximated by element-wise affine maps, i.e., we consider a displacement field $U_h \in \{u \in C(\Omega;\mathbb{R}^2);\ u \text{ is affine on each } \omega_i \in \mathcal{T}_h\}$ and the volume fraction $\boldsymbol{c}_h \in \{\boldsymbol{c} \in C(\Omega;\mathbb{R}^2);\ \boldsymbol{c} \text{ is affine on each } \omega_i \in \mathcal{T}_h\}$. The stored and dissipated energies are approximated using a two-dimensional trapezoidal rule, see e.g. [11]. As to the material properties we consider a very simple situation of a homogeneous isotropic material with Young modulus of 14 GPa and Poisson ratio of 0.3. We assume that $m = 2$ and take two tetragonal variants of martensite with $e^{1*} := \text{diag}(-0.05, 0.05)$ and $e^{2*} := \text{diag}(0.05, -0.05)$. We refer to e^{1*} as variant 1, or the white variant and to e^{2*} as variant 2, or the black variant. The two variants are mutually kinematically compatible, i.e.,

$$\begin{aligned} 2(e^{1*} - e^{2*}) &= (-0.1,-0.1) \otimes (1,-1) + (1,-1) \otimes (-0.1,-0.1) \\ &= (0.1,-0,1) \otimes (1,1) + (1,1) \otimes (0.1,-0,1)\ . \end{aligned}$$

Thus, strain discontinuities can be formed across interfaces between variants along the lines $x_1 - x_2 = 0$ or $x_1 + x_2 = 0$. We call this a 45-*degree interface*. As to the dissipation we set $|\boldsymbol{c}|_2 := \alpha_1|c_1| + \alpha_2|c_2|$ and allow for the possibility of a spatially variable penalty function $g(x)$ in (13).

The initial condition is such that always $c_1 = 1$, i.e. the whole specimen is in the variant e^{1*}. Spatially discretized incremental minimization problems (28) were solved by the L-BFGS-B routine described in [8].

5.1. **Strain-controlled experiments.** Our first example is a strain-controlled experiment, in which the magnitude of the phase-change penalty function is kept constant over the whole specimen at the value $g = 30\,\text{MPa}$. Zero Dirichlet boundary conditions prescribed in the x_2-direction on the boundary $(0,1) \times \{0\}$ and time-dependent Dirichlet boundary conditions on $(0,1) \times \{2\}$. In particular, the second component of the Dirichlet datum reads

$$u_{02}(t,x) = \begin{cases} 0.2 - 0.8t \text{ if } 0 \leq t \leq 0.5, \\ 0.2 + 0.8t - 0.8 \text{ if } 0.5 \leq t \leq 1\ . \end{cases} \tag{41}$$

We observe the formation of 45-degree interfaces across the specimen, as shown in Figure 1. Similar simulations were performed in [9], where the authors used a microscopic stored energy with a double well potential of the form $\tilde{W}(e) := \min((e-e^{1*})^2, (e-e^{2*})^2)$ without any interfacial energy term. This leads to spatial oscillations on the scale of the finite-element mesh.

In the next example, we consider a strain-controlled experiment with the same prescribed Dirichlet boundary conditions (41) as in the previous case, but with a phase-change penalty function $g : \Omega \to (0, +\infty)$ in (13) given by a randomly varying

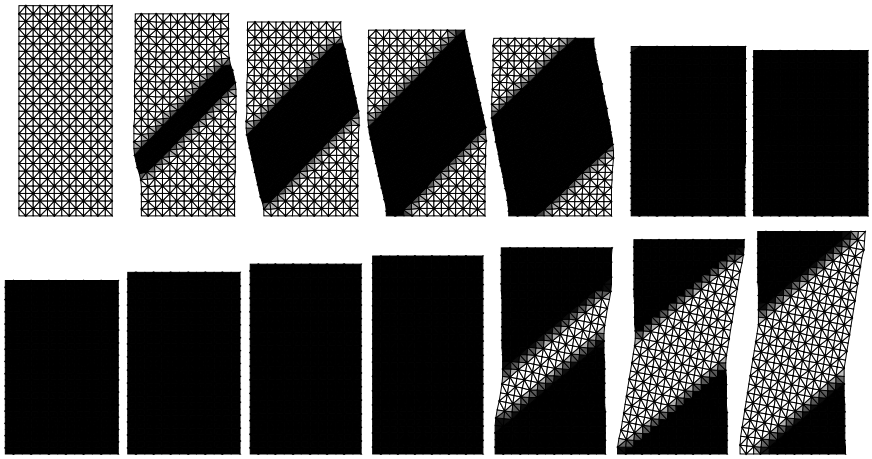

FIGURE 1. Nucleation of variant 2 (black) from variant 1 (white) in a specimen subject to cyclic Dirichlet boundary conditions (41) and spatially constant phase change penalty function $g = 30$ MPa. The displacement is 2x magnified and time increases from left to right in both rows.

distribution with values in the range between 18 MPa and 42 MPa, and average equal to 30 MPa. The results are shown in Fig. 2, and clearly suggest a competition between two effects. First, the transformation from e^{1*} to e^{2*} should start at $x \in \Omega$ whenever there is enough energy to overcome the penalty for phase change $g(x)$. Secondly, to keep the elastic energy $\mathcal{E}$ as small as possible the development of a 45-degree interface is necessary. A compromise between the two effects is achieved by a delayed nucleation of islands of black variant, with approximate 45-degree interfaces. This is clearly visible in Figure 2 which shows the evolution of the variants in the specimen. The upper row shows a few snapshots of the compression part, i.e. $t \in [0, 0.5]$, while the lower row shows the unloading program. The white color identifies variant 1 ($c_1 = 1$) and the black one variant 2 ($c_1 = 0$).

5.2. **Stress-controlled experiments.** A feature of our model is that it leads to a sudden transformation of the entire specimen in typical stress-controlled experiments if g and the initial volume fractions are spatially homogeneous. Indeed, consider the case $f = 0$ and $f_s = \Sigma\nu$ in (10) , where Σ is a second-order symmetric constant stress tensor and boundary conditions allowing for a homogeneous deformation. For example, consider an experiment where one presses the specimen against a lubricated support, along which the specimen can move "without" friction. Since we only consider two variants, i.e., $m = 2$ it is convenient to introduce a new variable $1 - c_1 =: \tilde{c} \in [0, 1]$ and put

$$c_1 e^{1*} + c_2 e^{2*} = c_1 e^{1*} + (1 - c_1) e^{2*} = e_1^* + \tilde{c}(e^{2*} - e^{1*}).$$

Moreover, the dissipation associated with a phase change from $\boldsymbol{c}$ (equal to either $(1, 0)$ for variant 1 or to $(0, 1)$ for variant 2) to $\boldsymbol{c}'$ (which is then equal to either $(0, 1)$ or to $(1, 0)$, respectively), is

$$g\left(\alpha_1 |c_1' - c_1| + \alpha_2 |c_2' - c_2|\right) = g(\alpha_1 + \alpha_2) = g\,, \tag{42}$$

where we have set $\alpha_1 + \alpha_2 = 1$ without loss of generality.

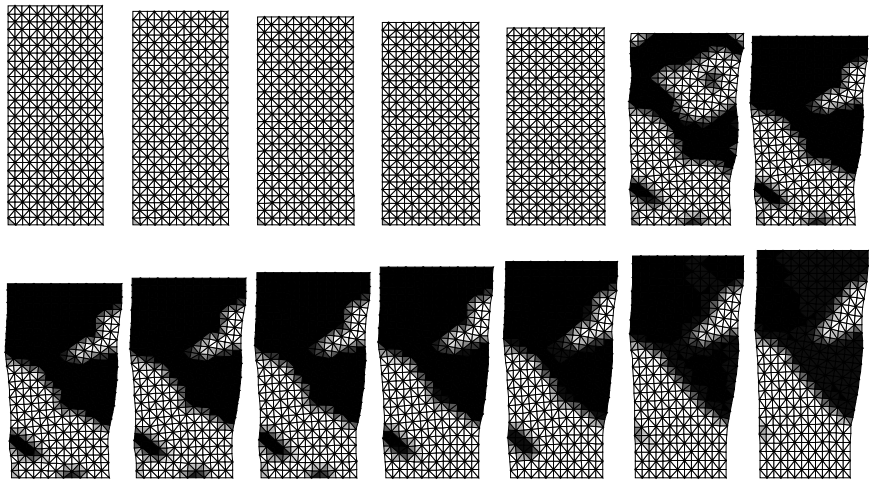

FIGURE 2. Nucleation of variant 2 (black) from variant 1 (white) in a specimen subject to cyclic Dirichlet boundary conditions (41) and heterogeneous, randomly varying phase change penalty function $g = 30 \pm 12$ MPa. The displacement is 2x magnified and time increases from left to right in both rows.

From (34) we have that, for a specimen which is initially in a homogeneous state, the transformation proceeds if

$$\Sigma \cdot (e^{2*} - e^{1*}) + \frac{1}{\varepsilon} \frac{\partial \Phi(\tilde{c})}{\partial \tilde{c}} + 2\varepsilon \Delta \tilde{c} = \pm g \ , \tag{43}$$

with the + sign holding for the transformation from variant 1 to 2, and − sign for the reverse transformation. Hence, if no interfacial energy is considered, i.e., $\varepsilon = 0$ and $\Phi = 0$, then the specimen transforms if $|\Sigma \cdot (e^{2*} - e^{1*})| = g$. However, the same happens if we consider the interfacial energy. Indeed, $\nabla \tilde{c} = 0$ for a spatially constant $\tilde{c}$. Moreover, $\tilde{c} \in \{0, 1\}$ is always energetically favorable because this does not increase the bulk elastic energy but decreases the energy coming from the Φ-term. This shows that, in the case of stress-controlled experiments on perfectly homogeneous samples, there will always be a sudden transformation of the entire specimen at

$$\Sigma \cdot (e^{2*} - e^{1*}) = \pm g \, . \tag{44}$$

In a plot of volume fraction versus applied stresses, such as the one given in Figure 5 below, the width of the resulting hysteresis loop would be proportional to $2g$, with sudden transformations at the critical loads.

The following example shows that, when a spatially varying phase change penalty is present, there can be nucleation of islands of a new phase in a stress-controlled experiment, with approximate 45 degree interfaces separating the pre-existing martensitic variant and the newly formed domains containing a different variant. This example is modeled after an experiment reported in [26] on biaxial loading of a CuAlNi specimen. We take a square specimen which is loaded by the stress $\Sigma = \mathrm{diag}(\sigma_1, \sigma_2)$

such that $\sigma_1 + \sigma_2 = -60$MPa and

$$\sigma_2(t) = \begin{cases} -120t & \text{if } 0 \le t \le 1/2 \\ 120t - 120 & \text{if } 1/2 \le t \le 1. \end{cases} \tag{45}$$

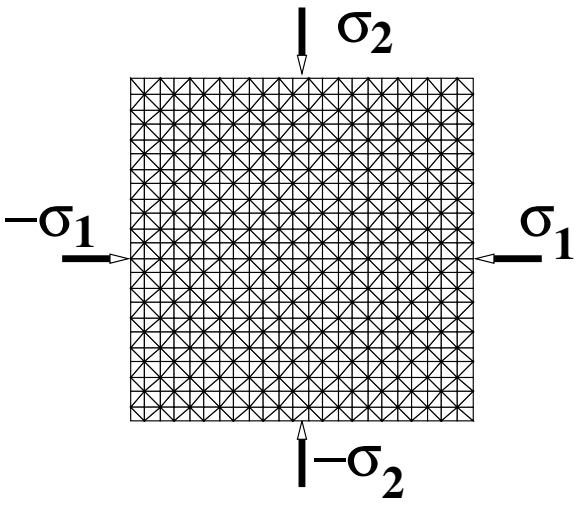

FIGURE 3. The square specimen, its discretization, and the applied surface forces, see (45).

The specimen and the loading conditions are depicted in Figure 3. The phase-change penalty function g is given by a randomly varying distribution with values in the range between 18 MPa and 42 MPa, and average equal to 30 MPa. Figure 4 shows the deformation of the specimen for $t \in [0, 0.5]$ (the first row) and for $t \in [0.5, 1]$ in the second one. Black color denotes variant 2 (i.e., e^{2*}), while the white one denotes variant 1 (i.e., e^{1*}). We see that the interfacial energy term favors 45 degree interfaces which are clearly visible during the creation and annihilation of black and white variants. Figure 5 shows a plot of the evolution of the volume fraction of variant 2 (i.e., e^{2*}) versus loading parameter $\frac{\sigma_1-\sigma_2}{\sigma_1+\sigma_2}$. The presence of defects and heterogeneities (described trough the random fluctuations of the phase-change penalty function g) reduces substantially the width of the hysteresis loop with respect to the case of constant $g = 30$ MPa, when this width would be $2g/(\sigma_1 + \sigma_2) = 1$, see (44).

In a final example we consider an elongated specimen, which is initially in a uniform state corresponding to variant 1, under a purely uniaxial loading acting along the long axis varying in the range ± 60 MPa, and favoring a transformation to variant 2. The phase-change penalty function g is given again by a randomly varying distribution with values in the range between 18 MPa and 42 MPa, and average equal to 30 MPa. This results in the fact that the specimen does not transform at once from a uniform state in pure variant 1 (white) to pure variant 2 (black), see Figure 6. Instead, we observe two competing trends. The first one is that the parts where the phase-change penalty is lower prefer to transform earlier, the second one is that the interfacial energy contribution favors 45 degree interfaces between variants. This results in a behavior similar to the one that is experimentally observed: starting

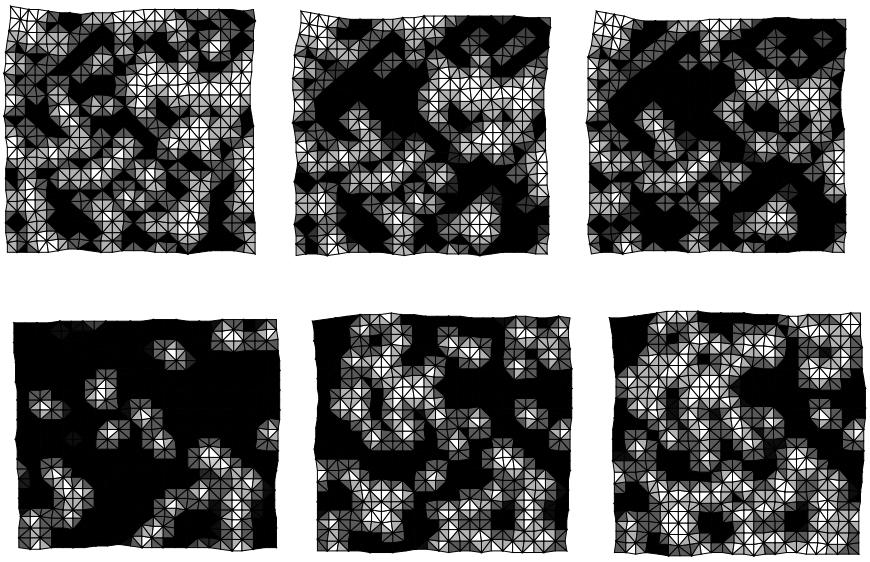

FIGURE 4. Nucleation of variant 2 (black) from variant 1 (white) in a stress-controlled experiment with a heterogeneous, randomly varying phase change penalty function $g = 30 \pm 12$ MPa. Surface tractions are $\sigma_1(t) + \sigma_2(t) = -60$MPa, and $\sigma_2(t)$ as in (45). The loading increases from left to right in the first row of snapshots and decreases in the second row.

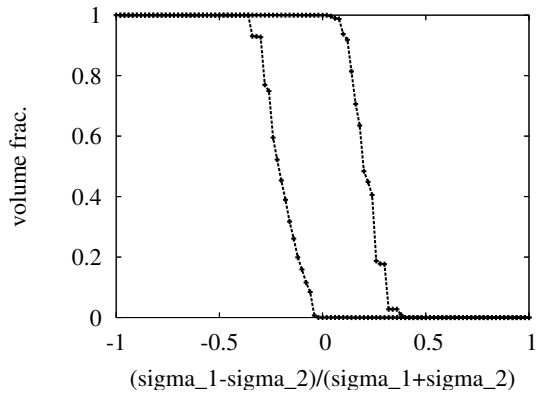

FIGURE 5. Volume fraction of variant 2 (i.e., e^{2*}) versus loading parameter $\frac{\sigma_1-\sigma_2}{\sigma_1+\sigma_2}$ in a stress-controlled experiment with a heterogeneous, randomly varying phase change penalty function $g = 30 \pm 12$ MPa. Surface tractions are $\sigma_1(t) + \sigma_2(t) = -60$MPa, and $\sigma_2(t)$ as in (45), i.e., the process starts at one on the horizontal axis and follows the loop clockwise.

from one variant (white) we observe an increasing number of black islands, with growing 45 degree interfaces between the black and white domains.

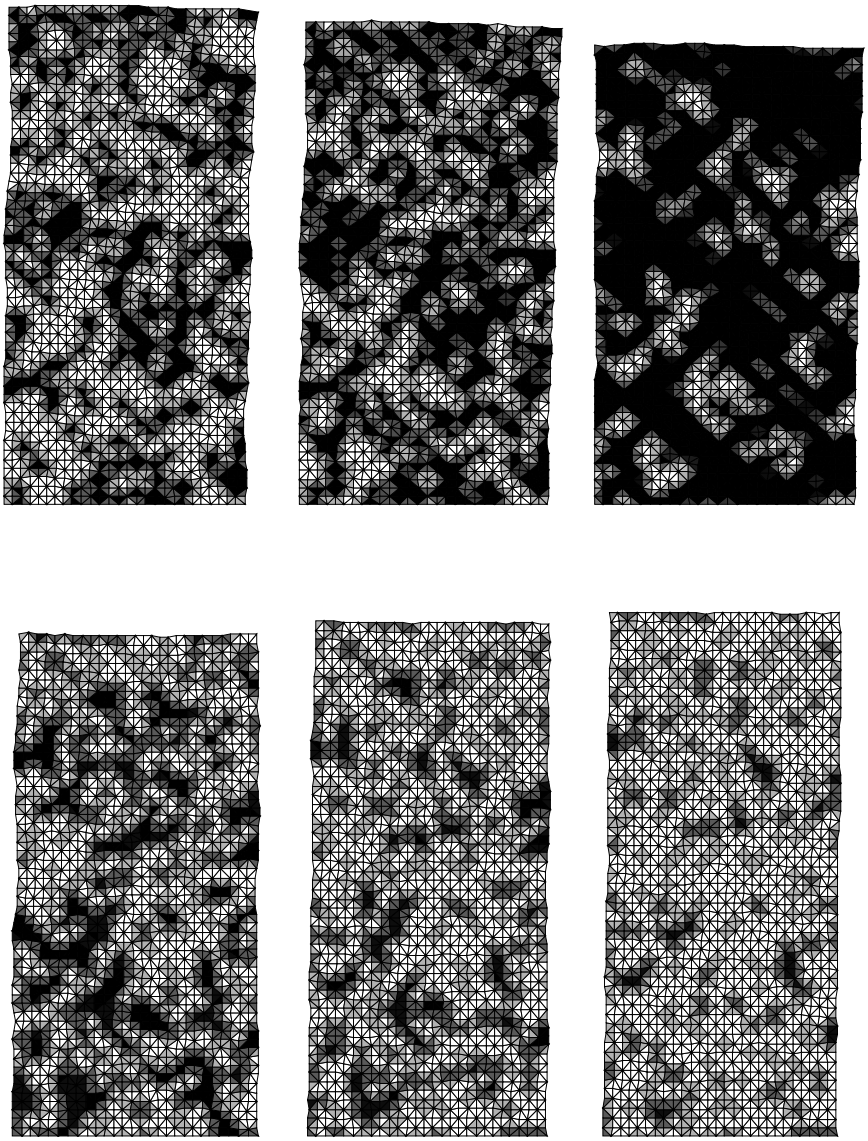

FIGURE 6. Nucleation of variant 2 (black) from variant 1 (white) under vertical uniaxial loading with a heterogeneous, randomly varying phase change penalty function $g = 30 \pm 12$ MPa. Surface tractions are $\sigma_1(t) = 0$ and $\sigma_2(t)$ varying in the range ± 60 MPa. The loading increases from left to right in the first row of snapshots and decreases in the second row.

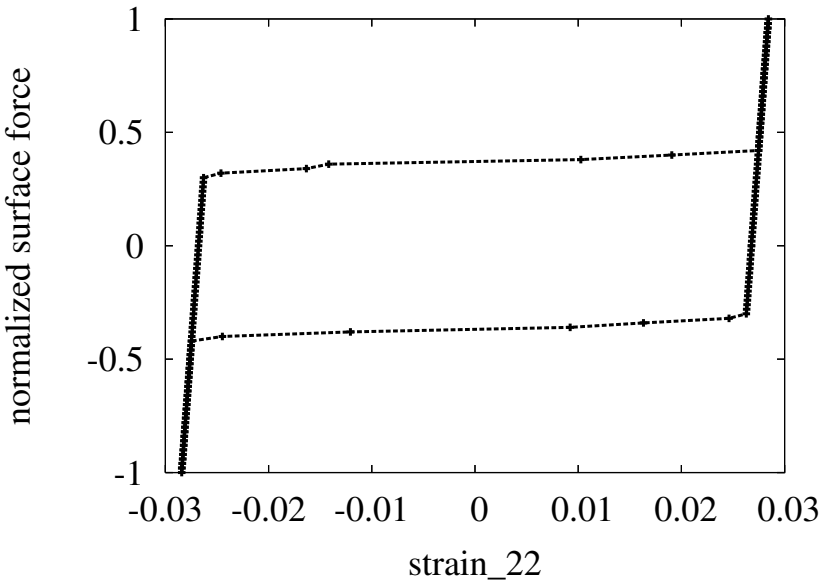

FIGURE 7. Stress–strain diagram for the uniaxial loading with a heterogeneous, randomly varying phase change penalty function $g = 30 \pm 12$ MPa, and $\sigma_1(t) = 0$ and $\sigma_2(t)$ varying in the range ± 60 MPa. The normalized surface force $\sigma_2(t)/60$ in the vertical axis is plotted against the 22 component of the average strain in the specimen.

Acknowledgments. This work was conceived and completed during visits of M.K. at SISSA and of A.D.S. at ÚTIA AV ČR. The support and hospitality of these two institutions are gratefully acknowledged. M.K. was further partly supported by the grant P201/12/0671(GA ČR).

REFERENCES

[1] G. Alberti and A. DeSimone, *Quasistatic evolution of sessile drops and contact angle hysteresis*, Arch. Rat. Mech. Anal., **202** (2011), 295–348.

[2] L. Ambrosio, *Metric space valued functions of bounded variations*, Ann. Scuola Normale Sup. Pisa Cl. Sci. (4), **17** (1990), 439–478.

[3] S. Baldo, *Minimal interface criterion for phase transitions in mixtures of Cahn-Hilliard fluids*, Ann. Inst. H. Poincaré Anal. Non Linéaire, **7** (1990), 67–90.

[4] S. Baldo and G. Belletini, Γ*-convergence and numerical analysis: An application to the minimal partition problem*, Ricerche Mat., **40** (1991), 33–64.

[5] H. Ben Belgacem, S. Conti, A. DeSimone and S. Müller, *Rigorous bounds for the Föppl-von Kármán theory of isotropically compressed plates*, Journal of Nonlinear Science, **10** (2000), 661–683.

[6] B. Benešová, *Global optimization numerical strategies for rate-independent processes*, J. Global Optim., **50** (2011), 197–220.

[7] W. F. Brown, *Virtues and weaknesses of the domain concept*, Revs. Mod. Physics, **17** (1945), 15–19.

[8] R. H. Byrd, P. Lu, J. Nocedal and C. Zhu, *A limited memory algorithm for bound constrained optimization*, SIAM J. Scientific Computing, **16** (1995), 1190–1208.

[9] C. Collins, D. Kinderlehrer and M. Luskin, *Numerical approximation of the solution of a variational problem with a double well potential*, SIAM J. Num. Anal., **28** (1991), 321–332.

[10] R. Conti, C. Tamagnini and A. DeSimone, *Critical softening in Cam-Clay plasticity: Adaptive viscous regularization, dilated time and numerical integration across stress-strain jump discontinuities*, Comput. Methods Appl. Mech. Engrg., **258** (2013), 118–133.
[11] J. Cooper, "Working Analysis," Elsevier Academic Press, 2005.
[12] G. Dal Maso, "An Introduction to Γ-Convegence," Progress in Nonlinear Differential Equations and their Applications, **8**, Birkhäuser Boston, Inc., Boston, MA, 1993.
[13] G. Dal Maso and A. DeSimone, *Quasistatic evolution for Cam-Clay plasticity: Examples of spatially homogeneous solutions*, Math. Model. Meth. Appl. Sci., **19** (2009), 1643–1711.
[14] G. Dal Maso, A. DeSimone, M. G. Mora and M. Morini, *A vanishing viscosity approach to quasistatic evolution in plasticity with softening*, Arch. Rat. Mech. Anal., **189** (2008), 469–544.
[15] G. Dal Maso, A. DeSimone and F. Solombrino, *Quasistatic evolution for Cam-Clay plasticity: A weak formulation via viscoplastic regularization and time rescaling*, Calc. Var. PDE, **40** (2011), 125–181.
[16] G. Dal Maso, A. DeSimone and F. Solombrino, *Quasistatic evolution for Cam-Clay plasticity: properties of the viscosity solutions*, Calc. Var. PDE, **44** (2012), 495–541.
[17] R. Delville, R. D. James, U. Salman, A. Finel and D. Schryvers, *Transmission electron microscopy study of low-hysteresis shape memory alloys*, in "Proceedings of ESOMAT 2009," 2009.
[18] A. DeSimone, *Hysteresis and imperfection sensitivity in small ferromagnetic particles*, Meccanica, **30** (1995), 591–603.
[19] A. DeSimone, N. Grunewald and F. Otto, *A new model for contact angle hysteresis*, Netw. Heterog. Media, **2** (2007), 211–225.
[20] A. DeSimone and L. Teresi, *Elastic energies for nematic elastomers*, Europ. Phys. J. E, **29** (2009), 191–204.
[21] L. C. Evans and R. F. Gariepy, "Measure Theory and Fine Properties of Functions," Studies in Advanced Mathematics, CRC Press, Boca Raton, FL, 1992.
[22] H. Garcke, "On Mathematical Models for Phase Separation in Elastically Stressed Solids," Habilitation Thesis, University of Bonn, Bonn, 2000.
[23] P. Germain, Q. Nguyen and P. Suquet, *Continuum thermodynamics*, J. Applied Mechanics, **50** (1983), 1010–1020.
[24] L. Fedeli, A. Turco and A. DeSimone, *Metastable equilibria of capillary drops on solid surfaces: A phase field approach,* Cont. Mech. Thermodyn., **23** (2011), 453–471.
[25] G. Francfort and A. Mielke, *Existence results for a class of rate-independent material models with nonconvex elastic energies*, J. Reine Angew. Math., **595** (2006), 55–91.
[26] R. D. James, *Hysteresis in phase transformations*, in "ICIAM 95" (Hamburg, 1995), Math. Res., **87**, Akademie Verlag, Berlin, (1996), 133–154.
[27] L. Juhász, H. Andrä and O. Hesebeck, *A simple model for shape memory alloys under multiaxial non-proportional loading*, in "Smart Materials" (ed. K.-H. Hoffmann), Proceedings of the 1st Caesarium, Springer, Berlin, (2000), 51–66.
[28] M. Kružík and M. Luskin, *The computation of martensitic microstructure with piecewise laminates*, Journal of Scientific Computing, **19** (2003), 293–308.
[29] M. Kružík, A. Mielke and T. Roubíček, *Modelling of microstructure and its evolution in shape-memory-alloy single-crystals, in particular in CuAlNi*, Meccanica, **40** (2005), 389–418.
[30] M. Kružík and F. Otto, *A phenomenological model for hysteresis in polycrystalline shape memory alloys*, ZAMM Z. Angew. Math. Mech., **84** (2004), 835–842.
[31] S. Leclerq, G. Bourbon and C. Lexcellent, *Plasticity like model of martensite phase transition in shape memory alloys*, J. Physique IV France, **5** (1995), 513–518.
[32] S. Leclerq and C. Lexcellent, *A general macroscopic description of thermomechanical behavior of shape memory alloys*, J. Mech. Phys. Solids, **44** (1996), 953–980.
[33] C. Lexcellent, S. Moyne, A. Ishida and S. Miyazaki, *Deformation behavior associated with stress-induced martensitic transformation in Ti-Ni thin films and their thermodynamical modelling*, Thin Solid Films, **324** (1998), 184–189.
[34] A. Mielke, T. Roubíček and U. Stefanelli, *Γ-limits and relaxations for rate-independent evolutionary problems*, Calc. Var., **31** (2008), 387–416.
[35] A. Mielke and F. Theil, *Mathematical model for rate-independent phase transformations*, in "Proceedings of the Workshop on Models of Continuum Mechanics in Analysis and Engineering" (eds. H.-D. Alber, R. Balean and R. Farwig), Shaker-Verlag, Aachen, (1999), 117–129.

[36] A. Mielke and F. Theil, *On rate-independent hysteresis models*, Nonlin. Diff. Eq. Appl., **11** (2004), 151–189.
[37] A. Mielke, F. Theil and V. Levitas, *A variational formulation of rate-independent phase transformations using extremum principle,* Arch. Rat. Mech. Anal., **162** (2002), 137–177.
[38] I. Müller, *Modelling and simulation of phase transition in shape memory metals*, in "Smart Materials" (ed. K.-H. Hoffmann), Proceedings of the 1st Caesarium, Springer, Berlin, (2000), 97–114.
[39] F. Nishimura, T. Hayashi, C. Lexcellent and K. Tanaka, *Phenomenological analysis of subloops and cyclic behavior in shape memory alloys under mechanical and/or thermal loads*, Mech. of Mat., **19** (1995), 281–292.
[40] T. Roubíček, *Evolution model for martensitic phase transformation in shape-memory alloys*, Interfaces and Free Boundaries, **4** (2002), 111–136.
[41] Y. C. Shu and J. H. Yen, *Multivariant model of martensitic microstructure in thin films*, Acta Materialia, **56** (2008), 3969–3981.
[42] M. Thomas, *Quasistatic damage evolution with spatial BV-regularization*, Discr. Cont. Dyn. Syst. Ser. S, **6** (2013), 235–255.
[43] J. M. T. Thomson and G. W. Hunt, "Elastic Instability Phenomena," J. Wiley and Sons, Chichester, 1984.

Received October 2012; revised March 2013.

E-mail address: desimone@sissa.it
E-mail address: kruzik@utia.cas.cz